*Desalination and Water Treatment*
www.deswater.com

doi: 10.5004/dwt.2022.28872

273 (2022) 236–245
October

# Adsorption efficiency of malachite green dye (MG) using a novel composite adsorbent based on synthesized alumina/acid-activated clay

Fatima Zohra Soufal[a], Abdelhafid Zehhaf[a,*], Bendoukha Abdelkrim Reguig[b], Faiza Chouli[b]

[a]*Laboratory of Process Engineering and Chemistry Solution, Department of Process Engineering, Faculty of Science and Technologies, Mascara University, BP 763, 29000 Mascara, Algeria, emails: a.zehhaf@univ-mascara.dz (A. Zehhaf), fatimaz.soufal@univ-mascara.dz (F.Z. Soufal)*
[b]*Laboratory of Organic, Macromolecular Chemistry and Materials, Department of Chemistry, Faculty of Exact Sciences, Mascara University, BP 763, 29000 Mascara, Algeria, emails: abdelkrim.reguig@univ-mascara.dz (B.A. Reguig), Chouli.faiza@univ-mascara.dz (F. Chouli)*

Received 29 May 2022; Accepted 21 August 2022

**ABSTRACT**

Our study aims to prepare a novel composite adsorbent via physical mixing process by using synthesized alumina from alum with acid activated clay (Alumina/H$^+$Clay) and estimate their efficiency for malachite green dye (MG) adsorption. The characterization of Alumina/H$^+$Clay composite was performed using various analyses techniques such as XRD, FT-IR, SEM, surface area analysis (BET), and $pH_{pzc}$. Furthermore, the effects of pH dye solution, adsorbent mass, initial concentration, and contact time on the adsorption process were investigated. Our results demonstrated that the prepared Alumina/H$^+$Clay composite is a mesoporous material with a pore volume and specific surface area of 0.58 $cm^3/g$, 89.02 $m^2/g$ respectively. The experimental data fit well with Langmuir isotherm with a maximum adsorption capacity of 243.06 mg/g. In addition, the kinetic parameters showed that the adsorption of MG dye followed the pseudo-second-order model. The obtained thermodynamic parameters indicated that the adsorption occurred spontaneously at different temperatures and the process was endothermic. Therefore, this study demonstrated that prepared Alumina/H$^+$Clay composite is an excellent adsorbent for MG dye and it could be used as an effective and promising adsorbent material for dyes.

*Keywords:* Adsorption; Malachite green; cationic dye; Wastewater; Composite material; Alumina/H$^+$Clay

## 1. Introduction

The industrial sector witnessed recently an intensive demand of various types of dyes as direct, reactive, acid, basic, disperse, vat, and sulfur dyes [1]. Indeed, 100,000 types of dyes and pigments are produced, and over $7 \times 10^5$ tons of synthetic dyes are annually supplied color processing market [2]. However, the aquatic environment is receiving about 7% of the effluents from the dye manufacturing, 8% from the paint industry and tannery, 10% from the paper and pulp industry, 21% from the dyeing industry, and a significant ratio from the textile industry estimated as 54% [3]. In addition, these dye effluents are contaminated with high levels of hazardous chemicals and their auxiliary products.

Among dyes, malachite green (MG), a triphenylmethane cationic dye used in the dyeing process (leather, wool, and silk), food processing, and treatment for fungal, and protozoal infections [4]. However, synthetic dyes can result in significant health issues, including child hyperactivity,

* Corresponding author.

allergies, and skin cancer [5]. In particular, various concerns have been demonstrated regarding the toxicity of malachite green dye as teratogenic and carcinogenic effects, which can threaten human life [6,7]. Besides, the discharge of malachite green dye in the hydrosphere decreases photosynthesis and affects aquatic plants [8].

It has been reported that the removal of malachite green has been explored by various technologies such as biological treatment (fungal species, bioluminescent bacterium) [9,10], chemical treatment (photocatalytic degradation [11], electrochemical oxidation [12]), and physical treatment (membrane filtration [13], ion exchange [14], and adsorption process [15]). Considering this, the adsorption process has been regarded as an effective, and suitable method for the removal of various pollutants owing to the low energy cost, and simple equipment manipulation [16]. In addition, the adsorption removal technology involves no undesirable toxic effects on the aquatic environment, and the adsorbent can be reused for further cycles [17,18].

Various kinds of adsorbents have been applied for malachite green dye removal as modified pine cone [19], *Curcuma caesia*-based activated carbon [20], synthetic hematite iron oxide nanoparticles [21], natural red clay [22], modified nano-γ-alumina [23], and graphene [24].

Among the listed adsorbents; alumina was recognized as a promising adsorbent with no toxicity, low cost, and excellent physicochemical properties such as high thermal stability and high specific surface area [25,26]. For instance, the adsorption of methylene blue and crystal violet dyes onto synthesized alumina via precipitation and calcination method using aluminum waste (51.81 and 31.92 mg/g respectively) [27], commercial alumina for eriochrome black T and malachite green dye (45 and 13.49 mg/g respectively) [28,29], and synthesized alumina via sol–gel for reactive yellow and orange G (25 and 93.3 mg/g respectively) [30,31]. However, different kinds of synthesized alumina adsorbents have shown weak efficiency for various pollutants. Thus, in order to enhance their structural characteristics and adsorption performance, alumina composite adsorbents have received considerable attention from researchers as synthesized alumina-zirconia composite for methylene blue and congo red [32], prepared $Al_2O_3$/zeolite composite for CO molecules [33], γ-alumina and silica amorphous mixture for methylene blue [34], alumina-onion skin composite for heavy metals [35] and alumina/nano-graphite composite for chromium (III) and chromium (VI) ions [36].

The objective of our study is the preparation of composite adsorbent via a physical mixing process by using synthesized alumina (from alum) with acid activated local clay. Different analysis techniques were performed for the characterization of the adsorbent such as XRD, FT-IR, BET, SEM, and $pH_{PZC}$. Furthermore, the performance of the adsorption process of malachite green dye was analyzed using kinetic, adsorption isotherm, and thermodynamic studies.

## 2. Materials and methods

### 2.1. Materials

Malachite green dye was obtained from Merck®. Hydrochloric acid (HCl) and Sodium hydroxide (NaOH) were purchased from Sigma-Aldrich®.

Clay sample was collected in Maghnia in the west of Algeria as local raw material, and their chemical composition is presented in Table 1 [37].

### 2.2. Preparation of Alumina/$H^+$Clay composite

Alumina was prepared via the thermal decomposition method [25]. Small pieces of alum sample ($Al_2(SO_4)_3{\cdot}18H_2O$) were grinded with a crusher and put in a muffle furnace at 1,000°C for 15 min.

The clay sample was washed with distilled water, crushed for 20 min, and dried for 2 h at 105°C. Acid activated clay was prepared using the protocol reported in a previous study [38]. In brief, 20 g of clay was added to a flask containing 200 mL of $H_2SO_4$ (0.25M) and stirred for 3 h under refluxed heating. Thereafter, the activated clay ($H^+$Clay) was washed several times with distilled water to eliminate $SO_4^{2-}$, and dried at 105°C.

Alumina/$H^+$Clay composite adsorbent was prepared via the physical mixing process [39] following the modified method of [40]. Briefly, acid activated clay/25 wt.% alumina were mixed with a magnetic stirrer (1,200 rpm) in a flask containing 100 mL of distilled water for 3 h at 25°C. Thereafter, the suspension was filtered and dried at 105°C overnight. Finally, the obtained composite was grinded for 20 min, sieved and stored in a desiccator until used.

### 2.3. Alumina/$H^+$Clay composite characterization

The X-ray diffraction (XRD) analysis was performed using (Goniometer MiniFlex 300/600 diffracted beam mono: Bent – Detector: SC-70) diffractometer with measurement condition of ($\lambda$ Cu Kα = 1.54 radiation 40 Kv, 15 mA). The surface functional groups of Alumina/$H^+$Clay composite were detected using (Alpha-Bruker) FT-IR. The surface area measurement (BET), pore size, and pore volume were conducted from the adsorption–desorption of $N_2$ at 77 K using (Micromeritics 3Flex). The morphology surface of Alumina/$H^+$Clay composite was observed using scanning electron microscopy (SEM) (Quanta FEG250). The pH value of point zero charge ($pH_{PZC}$) was determined as reported in the common 'drift method' [41].

### 2.4. Adsorption experiment

The batch experiment system was performed for MG dye adsorption with different concentrations (50–450 mg/L). In an Erlenmeyer flask containing 50 mL of

Table 1
Composition (wt.%) of the used raw clay

| Composition (wt.%) | $SiO_2$ | $Al_2O_3$ | $Fe_2O_3$ | MgO | $K_2O$ | $TiO_2$ | MnO | $SO_3$ | $Na_2O$ | $P_2O_5$ | $CaO_3$ |
|---|---|---|---|---|---|---|---|---|---|---|---|
| Raw clay | 69.71 | 14.67 | 1.16 | 1.07 | 0.79 | 0.177 | 0.098 | 0.91 | 0.5 | 0.013 | 0.3 |

MG dye solution, 50 mg of the adsorbent was added and shaken at 10 rpm at 25°C. 1 mL of dye was withdrawn from the flask at different time intervals (0–5 h), diluted, and centrifuged for 5 min at 4,200 rpm. The dye concentration was determined by measuring the solution absorption at $\lambda_{max}$ of 617 nm using a (Hitachi U-3000) UV-visible spectrophotometer. The pH of the initial solution of MG dye was adjusted from 2 to 7 by adding 0.1 M HCl or 0.1 M NaOH solution. The thermodynamic study was performed at 298, 303, and 308 K.

## 3. Results and discussion

### 3.1. Adsorbent characterization

The XRD analysis of Alumina/H⁺Clay, H⁺Clay, and alumina are displayed in Fig. S1. The XRD pattern of alumina highlighted an amorphous structure. Besides, the peaks observed at 2θ = 37°, 45° and, 67° classified the alumina sample as γ-alumina [30,42]. For the XRD pattern of H⁺Clay composite, the main peaks were observed at 2θ = 8°, 20°, 26°, corresponding to the montmorillonite and the quartz phase [43]. For the XRD pattern of Alumina/H⁺Clay composite, it was observed a decrease in the intensity of the characteristic peaks of alumina due to the deposition of H⁺Clay.

Fig. 1 presents the FT-IR spectra of H⁺Clay, alumina, and Alumina/H⁺Clay composite before and after adsorption. H⁺Clay spectrum showed absorption bands at around 778 and 1,040 $cm^{-1}$ that attributed to Si–O as the main functional group presented in clay [44]. Besides, the peaks observed at 1,663 and 3,394 $cm^{-1}$ are attributed to O–H stretching vibration and H–O–H deformation vibration of water molecules respectively [43]. For alumina spectrum, the absorption bands located near 3,422 and 511 $cm^{-1}$ are assigned to the bending vibration of the –OH group and Al–O stretching vibration respectively [41]. Regarding the spectrum of Alumina/H⁺Clay composite, new absorption bands were appeared after the adsorption process. Indeed, the peaks observed at around 1,372 and 1,587 $cm^{-1}$, corresponding to the C=C stretching vibration of the benzene ring and C–C aromatic stretching presented in MG dye respectively [27].

The textural properties and the nitrogen sorption/desorption isotherms of Alumina/H⁺Clay composite and alumina are presented in Fig. 2. Based on the IUPAC classification of adsorption isotherm, Alumina/H⁺Clay composite and alumina were belonged to type-IV isotherms with H-3 hysteresis loop, suggesting that both samples had a variety of pore diameters [45,46]. Moreover, the pore diameter revealed that Alumina/H⁺Clay composite and alumina were classified as mesoporous materials [47]. The BET analysis showed a decrease of the specific surface area from 168 to 89.02 $m^2/g$ for alumina and Alumina/H⁺Clay composite, respectively. Similar findings were observed by other composite adsorbents demonstrated in the literature as clay/alumina composite [48], bentonite/γ-alumina composite [40], and aluminium/modified carbon [49]. The decrease in the specific surface area could be related to the occupation of alumina pores with H⁺Clay added and incorporated on their surface.

The SEM images of Alumina/H⁺Clay composite before and after MG dye adsorption are presented in Fig. S2. Our results indicated that the prepared Alumina/H⁺Clay composite had a heterogeneous and porous surface morphology (Fig. S2a). After the adsorption process (Fig. S2a), it was observed a change in the surface of the composite, indicating the adsorption of MG dye molecules onto Alumina/H⁺Clay surface.

The charge surface of the adsorbent is one of the significant parameters affecting the adsorption mechanism [50]. The $pH_{PZC}$ of Alumina/H⁺Clay composite is presented in Fig. 4. The $pH_{PZC}$ value of Alumina/H⁺Clay composite was found to be 7. Consequently, the adsorbent exhibited

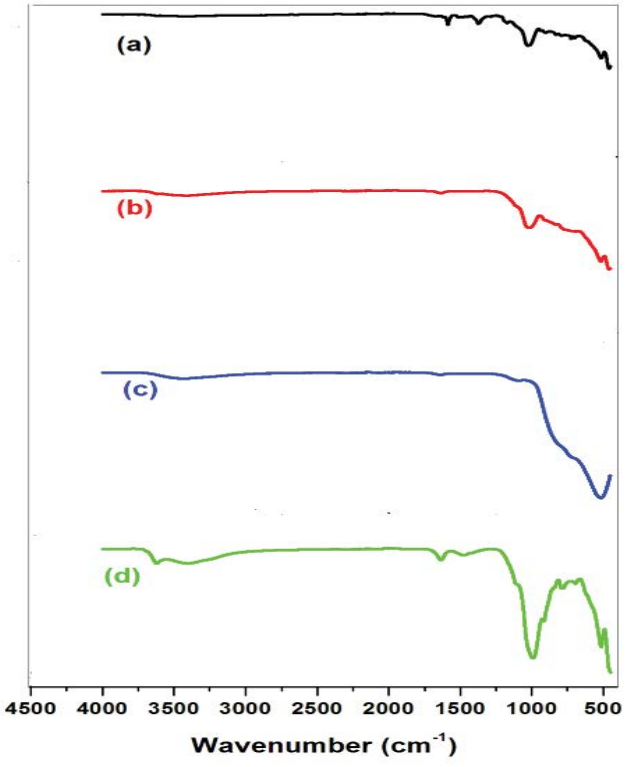


Fig. 1. FT-IR spectra of (a) H⁺Clay, (b) alumina, (c) Alumina/H⁺Clay composite before and (d) after MG dye adsorption.

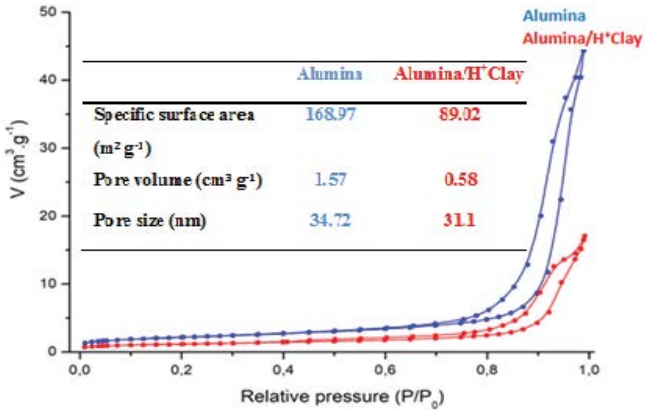


Fig. 2. Adsorption–desorption isotherms of alumina and Alumina/H⁺Clay composite.

dominantly a positive charge surface at pH < $pH_{PZC}$ and a negative charge at pH > $pH_{PZC}$. Similarly, the $pH_{PZC}$ of other adsorbents was found to be close to that of the Alumina/$H^+$Clay composite such as xanthan gum/$SiO_2$ composite ($pH_{PZC}$ = 6.2) [51], modified graphene ($pH_{PZC}$ = 7.33) [52] and fig opuntia derived activated carbon ($pH_{PZC}$ = 7.54) [53].

### 3.2. Adsorption study

To evaluate the removal efficiency of MG dye, a primary adsorption test was performed (under similar conditions) using raw clay, $H^+$Clay, alumina, and Alumina/$H^+$Clay composite. As shown in Fig. 3, MG dye removal efficiency using Alumina/$H^+$Clay composite exhibited a significant increase and reached a rapid equilibrium in the first 10 min, with a dye removal efficiency of 91.18% followed by acid activated clay (84.92%) and raw clay (79.12%). However, alumina adsorbent showed only 46.49% of MG dye removal percentage and reached equilibrium after 2 h. These primary results suggested that the prepared Alumina/$H^+$Clay composite had a higher affinity with MG dye.

The pH value of dye solution is a notable parameter that affects the adsorption process [54]. Fig. 4 presents the pH effect on the adsorption capacity of MG dye solution onto Alumina/$H^+$Clay composite. Since MG dye changes to a carbinol base at alkaline conditions (colorless) and protonated to $MGH^+$ under acidic conditions (cyan) [55], the pH effect was assessed in initial pH dye solution varies from 2 to 7. As shown in Fig. 4, the $pH_{PZC}$ of the Alumina/$H^+$Clay composite was 7 indicating that the adsorbent exhibited a positive charge surface at pH < $pH_{PZC}$. Besides, MG dye is positively charged due to the presence of the cationic $–NR_2$ groups. This means that both the adsorbent and adsorbate were positively charged. However, Alumina/$H^+$Clay composite exhibited a maximal adsorption capacity within the variation of pH dye solution. Similar behavior of MG dye was demonstrated by other scholars where the adsorption capacity of MG dye onto different adsorbents did not affect by the pH dye solution as apple seed/bentonite composite adsorbent, ball clay/manganese dioxide adsorbent, and polystyrene waste adsorbent [56–58]. This finding could be explained by the presence of other important contributions in the adsorption mechanism such as pore-filling which is the most common mechanism for metal oxide composites adsorbent [25].

The effect of the adsorbent mass of Alumina/$H^+$Clay on the adsorption capacity and MG dye removal is presented in Fig. 5. The results indicated that the MG dye removal rose sharply as the amount of the adsorbent increased from 25 to 50 mg. This can be related to the availability of active sites on the porous surface of the adsorbent [59]. Regarding the adsorption capacity of Alumina/$H^+$Clay composite, it was observed a decrease from 164.6 to 24.94 mg/g with an increase of the adsorbent mass from 25 to 200 mg respectively. These phenomena can be explained by the lack of MG dye molecules in the solution at a higher adsorbent amount [60]. Therefore, 50 mg was selected as the optimum adsorbent amount.

The effect of contact time on the adsorption capacity of MG dye adsorption onto Alumina/$H^+$Clay composite is presented in Fig. 6. The results showed a marked increase of

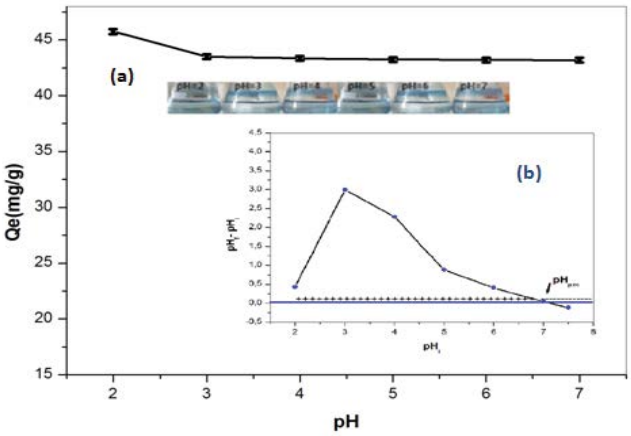


Fig. 4. (a) Effect of the pH dye solution on the adsorption of MG dye (100 mg/L, 0.1 g, 50 mL and 25°C) and (b) $pH_{pzc}$ of Alumina/$H^+$Clay.

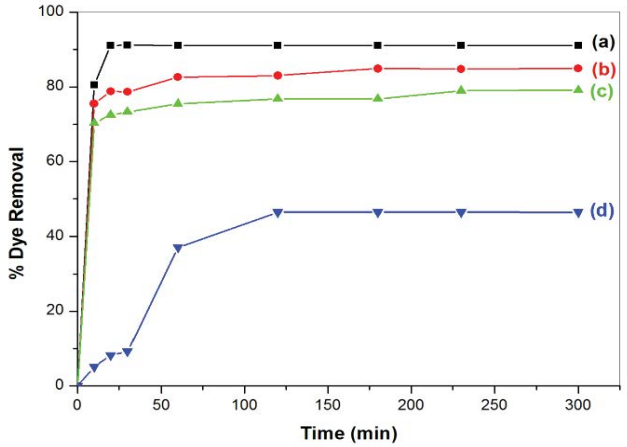


Fig. 3. Removal efficiency of MG dye using (a) Alumina/$H^+$Clay composite, (b) $H^+$Clay, raw clay (c) and (d) alumina (100 mg/L, 0.1 g, 50 mL and 25°C).

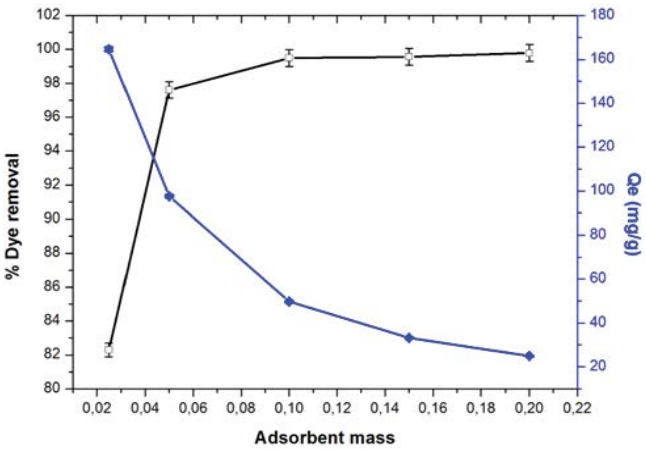


Fig. 5. Effect of Alumina/$H^+$Clay mass on the adsorption of MG dye (100 mg/L, 0.05–0.2 g, 50 mL and 25°C).

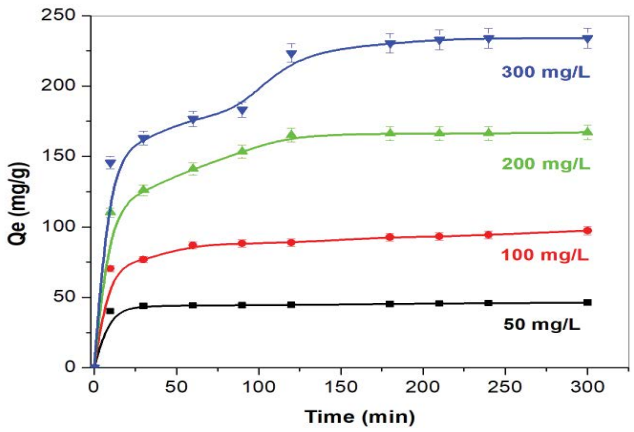


Fig. 6. Effect of contact time on the adsorption capacity of MG dye (0.05 g, 50 mL and 25°C).

the adsorption capacity in the first hour with approximately 70% of MG dye removal. Thereafter, a slight increase was recorded, and the adsorption process reached equilibrium at around 3h of contact time. This is could be explained by the availability of many vacant adsorption sites on the surface of Alumina/H⁺Clay composite at the initial contact time, and after the saturation of the empty sites by MG dye molecules, the adsorption rate decreased until the equilibrium was achieved [61,62]. Furthermore, the adsorption capacity elevated significantly from 46.32 to 234 mg/g with the increase of the initial concentration of MG dye from 50 to 300 mg/L respectively.

### 3.3. Adsorption kinetic study

The adsorption kinetic study plays a significant role in identifying and interpreting the kinetic data for the process of dye adsorption. For the adsorption of MG dye onto Alumina/H⁺Clay composite, we applied the non-linear forms of the pseudo-first-order model (1), and pseudo-second-order model (2) [63]:

$$q_t = q_e \times \left(1 - e^{-k_1 t}\right) \tag{1}$$

$$q_t = \frac{q_e^2 \times K_2 \times t}{1 + q_e \times K_2 \times t} \tag{2}$$

where $q_e$, $q_t$ (mg/g) are the adsorption capacity at time $t$, and at equilibrium respectively, $t$ (min) is the time, $K_1$, and $K_2$ are the rate constants of pseudo-first-order, and pseudo-second-order models respectively.

The fitted curves and the kinetic parameters are presented in Fig. 7, and Table 2, respectively. The results pointed out that the pseudo-second-order model was found to provide a better fit with a higher correlation coefficient ($R^2$) compared to the pseudo-first-order model. Consequently, this consistency suggested that both the physisorption and chemisorption control the adsorption process of MG dye onto Alumina/H⁺Clay composite [64].

### 3.4. Adsorption isotherm

The adsorption isotherms study is a significant step for interpreting the dye adsorption mechanism onto the adsorbent and estimating the maximum adsorption capacity. Fig. 8 presents the adsorption isotherm of MG dye using Alumina/H⁺Clay composite with initial concentrations (50 and 450 mg/L). Our results showed that the isotherm was an L-type isotherm shape, revealing that the Van Der Waals forces were involved in the adsorption mechanism [65].

For exploring the adsorption process of MG dye onto Alumina/H⁺Clay composite, we applied the non-linear forms of the adsorption isotherms of Langmuir (3) and Freundlich models (4) [66]:

$$q_e = \frac{q_m K_L C_e}{1 + K_L C_e}, \quad R_L = \frac{1}{1 + C_0 K_L} \tag{3}$$

$$q_e = K_f + C_1^{1/n_f} \tag{4}$$

where $K_L$ (L/mg), $K_f$ ((mg/g)/(mg/L)$^n$), are the constants of Langmuir, and Freundlich models respectively, $C_e$ (mg/L) is the equilibrium concentration of MG dye, $q_m$ (mg/g) is the maximum adsorption capacity, $q_e$ (mg/g) is equilibrium adsorption capacity, $C_0$ is the highest initial MG dye concentration (mg/L), $R_L$ is the separation factor, and $1/n$ is the intensity of adsorption constant.

Table 3 summarizes the calculated parameters of Langmuir and Freundlich isotherms. Our data indicated that the adsorption process of MG dye onto Alumina/H⁺Clay composite fitted better to the Freundlich model ($R^2 = 0.972$) than the Langmuir model ($R^2 = 0.925$). Moreover, the value of the $1/n_f$ ($0 < 1/4.66 < 1$) confirmed a favorable adsorption process of MG dye signifying the multi-layer adsorption and heterogeneity surface [67]. The maximum adsorption capacity of Alumina/H⁺Clay composite achieved 243.06 mg/g, demonstrating a higher adsorption capacity than other adsorbents used for MG dye (Table 4) [68–72]. Correspondingly, the prepared Alumina/H⁺Clay composite can serve as an effective and promising adsorbent for MG dye.

### 3.5. Thermodynamic study

The thermodynamic study was evaluated at different temperatures (from 298 to 318 K) for the adsorption of MG dye onto Alumina/H⁺Clay composite. The thermodynamic parameters: Gibbs free energy ($\Delta G°$), enthalpy ($\Delta H°$), and entropy change ($\Delta S°$), were calculated according to the following laws [73]:

$$\Delta G° = -RT \ln K_c \tag{5}$$

$$K_c = \frac{q_e}{C_e} \tag{6}$$

$$\ln K_c = -\Delta G° RT = \Delta S° - \frac{\Delta H}{RT} \tag{7}$$

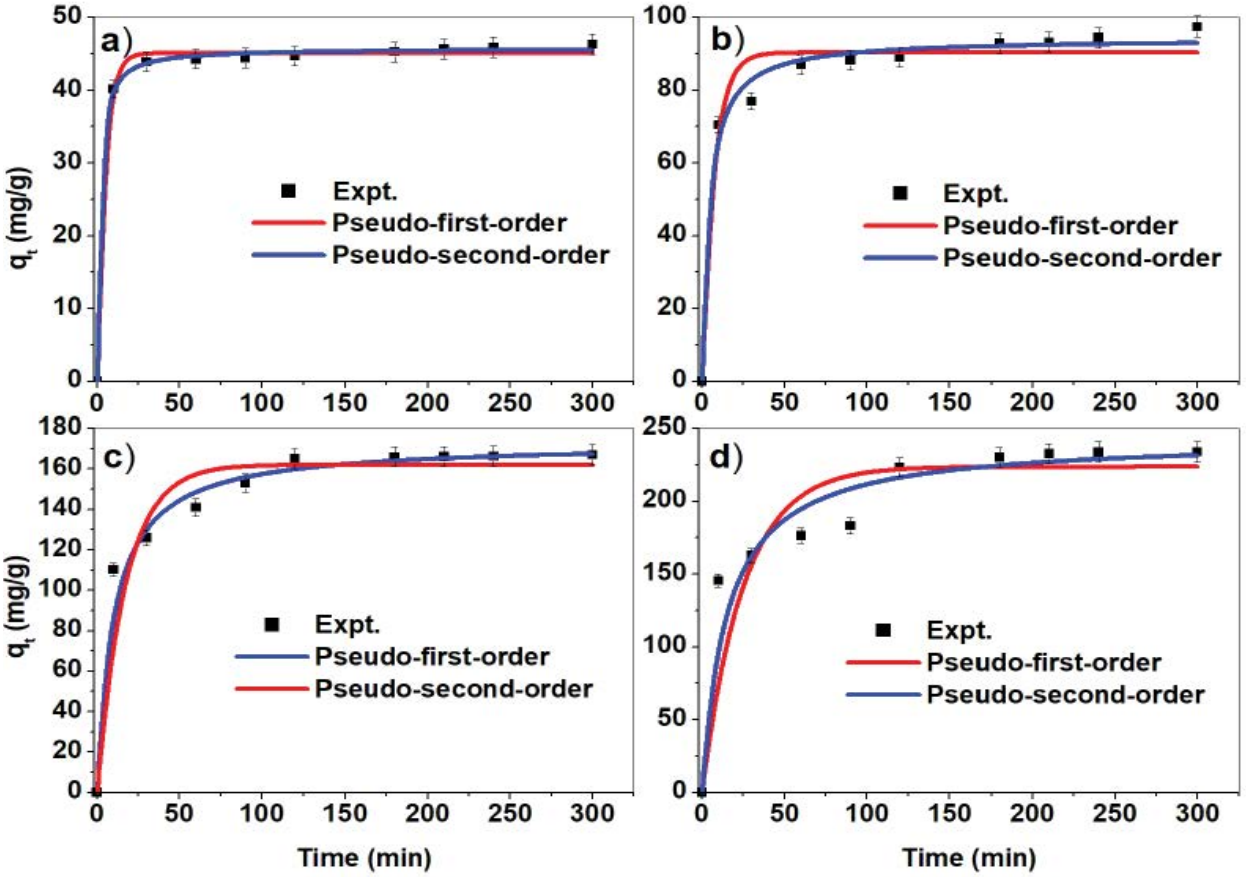


Fig. 7. Kinetic models fitting for MG dye adsorption onto Alumina/H⁺Clay for (a) 50 mg/L, (b) 100 mg/L, (c) 200 mg/L, and (d) 300 mg/L.

Table 2
Kinetic parameters of MG dye adsorption onto Alumina/H⁺Clay

| Models | Unit | Concentration | | | |
|---|---|---|---|---|---|
| | | 50 mg/L | 100 mg/L | 200 mg/L | 300 mg/L |
| Pseudo-first-order | | | | | |
| $Q_e$ (cal) | $Q_{e(exp)}$ | 45.075 | 90.311 | 162.02 | 223.17 |
| $Q_e$ (exp) | (mg/g) | 46.32 | 97.4 | 167 | 234 |
| $K_1$ | ($min^{-1}$) | 0.221 | 0.141 | 0.059 | 0.04 |
| $R^2$ | | 0.997 | 0.966 | 0.891 | 0.793 |
| Pseudo-second-order | | | | | |
| $Q_e$ (cal) | (mg/g) | 45.761 | 94.23 | 172.99 | 243.15 |
| $Q_e$ (exp) | (mg/g) | 46.32 | 97.4 | 167 | 234 |
| $K_2$ | (g/mg min) | 0.015 | 0.0026 | 0.0005 | 0.0002 |
| $R^2$ | | 0.999 | 0.989 | 0.971 | 0.993 |

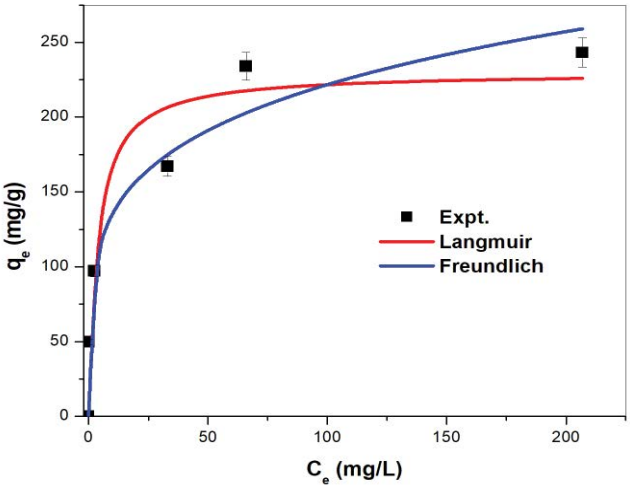


Fig. 8. Isotherm models fitting for MG dye adsorption onto Alumina/H⁺Clay.

where $R$ (8.314 J/mol·K) is the universal gas constant, $K_c$ (mg/L) is the concentration of compound at equilibrium, $q_e$ (mg/g) is the amount adsorbed at equilibrium at a particular temperature and $T$ (K) is the solution temperature.

The thermodynamic parameters are listed in Table 5. As revealed in Table 5, the negative values of $\Delta G°$ (–22.29, –23.29, and –23.7) pointed out that the adsorption process of MG dye was spontaneous. Furthermore, the positive value of $\Delta H°$ (37.25 kJ/ mol) demonstrated that the process was endothermic, and the adsorption process of

MG dye onto Alumina/H⁺Clay composite was mainly physisorption [74]. The positive values $\Delta S°$ revealed a randomness rising at the adsorbent–adsorbate interface during the adsorption process of MG dye [65].

### 3.6. Adsorbent regeneration study

To evaluate the reusability of Alumina/H⁺Clay composite for MG dye removal, a regeneration study was performed using a mixture of water and ethanol for four successive cycles ($C$ = 100 mg/L). As displayed in Fig. 9, the results indicated that Alumina/H⁺Clay composite highlights good reusability even after four desorption cycles, and the removal efficiency of MG dye was slightly decreased.

### 3.7. Adsorption mechanism

As previously highlighted in the FT-IR spectra of Alumina/H⁺Clay before and after adsorption (Fig. 1), new peaks were observed at around 1,372 and 1,587 $cm^{-1}$, indicating the adsorption of MG dye. Besides, It was observed the stretching vibration at 3,420 $cm^{-1}$ of the hydroxyl group (–OH) of Alumina/H⁺Clay composite was weakened, revealing hydrogen bonding between the nitrogen atoms of MG dye molecules and Alumina/H⁺Clay [75]. In addition, the contribution of van der Waals force and pores filling in the adsorption process of basic dyes has been demonstrated by various scholars as the adsorption of crystal violet [74], methylene green [76], methyl blue (MB), and basic fuchsin [77]. Taken together, the adsorption mechanism of MG dye onto Alumina/H⁺Clay could be explained by the combination of many contributors including pore filling, van der Waals force, and hydrogen bondings.

Table 3
Isotherm parameters of MG dye onto Alumina/H⁺Clay composite

| Langmuir | | Freundlich | |
|---|---|---|---|
| $Q_m$ (cal) (mg/g) | 229.94 | $K_f$ (mg/g)/(mg/L)$^n$ | 82.58 |
| $Q_m$ (exp) (mg/g) | 243.06 | | |
| $K_L$ (L/mg) | 0.267 | $n$ | 4.66 |
| $R_L$ | 0.012–0.069 | | |
| $R^2$ | 0.925 | $R^2$ | 0.972 |

## 4. Conclusion

Alumina/H⁺Clay composite was prepared using synthesized alumina and modified clay applied for MG dye adsorption. The main findings were:

- The textual analysis showed that the Alumina/H⁺Clay composite is a porous material with a specific surface area of 89.02 $m^2/g$.
- The optimum parameters for the adsorption of MG dye into alumina/H⁺-clay were: 3 h of contact time, 25°C and, 50 mg of adsorbent.
- The kinetic study demonstrated that the pseudo-second-order model described well the experimental data.
- The adsorption capacity of Alumina/H⁺Clay for MG dye was 243.06 mg/g at 25°C.

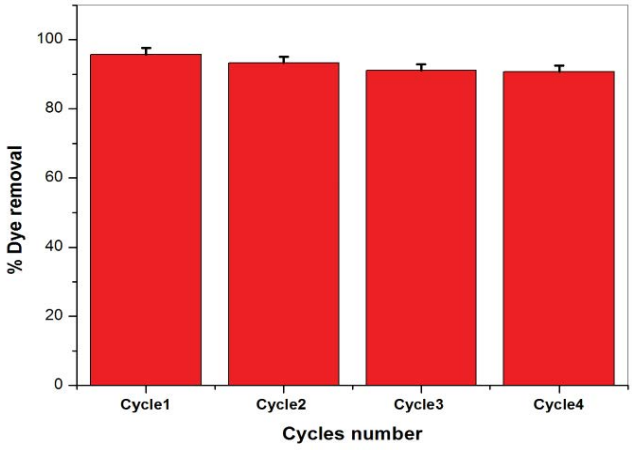


Fig. 9. Reusability of Alumina/H⁺Clay composite in MG dye adsorption.

Table 5
Thermodynamic parameters of MG dye adsorption onto Alumina/H⁺Clay composite.

| $T$ (K) | $\Delta G$ (kJ/mol) | $\Delta H$ (kJ/mol) | $\Delta S$ (J/mol·K) |
|---|---|---|---|
| 273 | –22.29 | 37.25 | 14.68 |
| 303 | –23.29 | | |
| 313 | –23.7 | | |

Table 4
Comparison of the maximum adsorption capacity of MG dye with other composite adsorbents

| Adsorbents | Maximum adsorption capacity (mg/g) | Reference |
|---|---|---|
| Zeolite/reduced graphene oxide | 48.6 | [68] |
| Magnetic metal organic frameworks | 113.67 | [69] |
| Fe2O3/Activated carbon | 36.36 | [70] |
| Commercial activated carbon (Coconut-AC, Coal-AC, Apricot-AC, Peach-AC) | 83, 74.91, 69.59, 69.93 | [71] |
| Activated carbon | 27 | [72] |
| Alumina/H+Clay | 243.06 | In this study |

- The thermodynamic parameters stated that the adsorption process of MG dye was spontaneous and endothermic.

Therefore, the prepared Alumina/$H^+$Clay composite could be considered an effective and promising adsorbent for cationic dyes.

## Acknowledgments

The authors wish to extend their special thanks to the Ministry for Higher Education for their supports for this research. Furthermore, a special thank to Prof. Fatima Zeggai (a researcher at CRPC) for her collaboration and effort.

## References

[1] S. Benkhaya, S. M'rabet, A. El Harfi, A review on classifications, recent synthesis and applications of textile dyes, Inorg. Chem. Commun., 115 (2020) 107891, doi: 10.1016/j.inoche.2020.107891.
[2] D. Bhatia, N.R. Sharma, J. Singh, R.S. Kanwar, Biological methods for textile dye removal from wastewater: a review, Crit. Rev. Env. Sci. Technol., 47 (2017) 1836–1876.
[3] S. De Gisi, G. Lofrano, M. Grassi, M. Notarnicola, Characteristics and adsorption capacities of low-cost sorbents for wastewater treatment: a review, Sustainable Mater.Technol., 9 (2016) 10–40.
[4] M. Santhi, P.E. Kumar, B. Muralidharan, Removal of malachite green dyes by adsorption onto activated carbon – $MnO_2$ – nanocomposite – kinetic study and equilibrium isotherm analyses, IOSR J. Appl. Chem. (IOSR-JAC), 8 (2015) 33–41.
[5] J. Mittal, Permissible synthetic food dyes in India, Resonance, 25 (2020) 567–577.
[6] A.S. Sartape, A.M. Mandhare, V.V. Jadhav, P.D. Raut, M.A. Anuse, S.S. Kolekar, Removal of malachite green dye from aqueous solution with adsorption technique using *Limonia acidissima* (wood apple) shell as low cost adsorbent, Arabian J. Chem., 10 (2017) S3229–S3238.
[7] S. Young, L. Berger, R. Speare, *Amphibian chytridiomycosis*: strategies for captive management and conservation, Int. Zoo Yearbook, 41 (2007) 85–95.
[8] N.P. Raval, P.U. Shah, N.K. Shah, Malachite green "a cationic dye" and its removal from aqueous solution by adsorption, Appl. Water Sci., 7 (2017) 3407–3445.
[9] T. Arunprasath, S. Sudalai, R. Meenatchi, K. Jeyavishnu, A. Arumugam, Biodegradation of triphenylmethane dye malachite green by a newly isolated fungus strain, Biocatal. Agric. Biotechnol., 17 (2019) 672–679.
[10] S.S. Sutar, P.J. Patil, A.S. Tamboli, D.N. Patil, O.A. Apine, J.P. Jadhav, Biodegradation and detoxification of malachite green by a newly isolated bioluminescent bacterium *Photobacterium leiognathi* strain MS under RSM optimized culture conditions, Biocatal. Agric. Biotechnol., 20 (2019) 101183, doi: 10.1016/j.bcab.2019.101183.
[11] D. Miao, G. Liu, Q. Wei, N. Hu, K. Zheng, C. Zhu, T. Liu, K. Zhou, Z. Yu, L. Ma, Electro-activated persulfate oxidation of malachite green by boron-doped diamond (BDD) anode: effect of degradation process parameters, Water Sci. Technol., 81 (2020) 925–935.
[12] R. Parvarideh, A.A. Aghapour, S.J. Jafari, S. Karimzadeh, H. Khorsandi, A comparison of single and catalytic ozonation for decolorization of malachite green, Desal. Water Treat., 152 (2019) 411–418.
[13] I. Ali, C. Peng, I. Naz, D. Lin, D.P. Saroj, M. Ali, Development and application of novel bio-magnetic membrane capsules for the removal of the cationic dye malachite green in wastewater treatment, RSC Adv., 9 (2019) 3625–3646.
[14] G. Sharma, V.K. Gupta, S. Agarwal, A. Kumar, S. Thakur, D. Pathania, Fabrication and characterization of Fe@MoPO nanoparticles: ion exchange behavior and photocatalytic activity against malachite green, J. Mol. Liq., 219 (2016) 1137–1143.
[15] S. Kaur, R. Jindal, J. Kaur Bhatia, Synthesis and RSM-CCD optimization of microwave-induced green interpenetrating network hydrogel adsorbent based on gum copal for selective removal of malachite green from waste water, Polym. Eng. Sci., 58 (2018) 2293–2303.
[16] H.M. Mbuvi, Adsorption kinetics and isotherms of methylene blue by geopolymers derived from common clay and rice husk ash, Phys. Chem., 7 (2017) 87–97.
[17] A. Mittal, J. Mittal, Chapter 11 – Hen Feather: A Remarkable Adsorbent for Dye Removal, S.K. Sharma, Ed., Green Chemistry for Dyes Removal from Wastewater: Research Trends and Applications, Scrivener Publishing LLC, USA, 2015, pp. 409–457.
[18] R. Jain, P. Sharma, S. Sikarwar, J. Mittal, D. Pathak, Adsorption kinetics and thermodynamics of hazardous dye Tropaeoline 000 unto Aeroxide Alu C (Nano alumina): a non-carbon adsorbent, Desal. Water Treat., 52 (2014) 7776–7783.
[19] E. Kavci, Malachite green adsorption onto modified pine cone: isotherms, kinetics and thermodynamics mechanism, Chem. Eng. Commun., 208 (2021) 318–327.
[20] C. Arora, P. Kumar, S. Soni, J. Mittal, A. Mittal, B. Singh, Efficient removal of malachite green dye from aqueous solution using *Curcuma caesia* based activated carbon, Desal. Water Treat., 195 (2020) 341–352.
[21] A. Dehbi, Y. Dehmani, H. Omari, A. Lammini, K. Elazhari, A. Abdallaoui, Hematite iron oxide nanoparticles ($\alpha$-$Fe_2O_3$): synthesis and modelling adsorption of malachite green, J. Environ. Chem. Eng., 8 (2020) 103394, doi: 10.1016/j.jece.2019.103394.
[22] F. Sevim, O. Lacin, E.F. Ediz, F. Demir, Adsorption capacity, isotherm, kinetic, and thermodynamic studies on adsorption behavior of malachite green onto natural red clay, Environ. Prog. Sustainable Energy, 40 (2021) e13471, doi: 10.1002/ep.13471.
[23] E. Mohammadifar, F. Shemirani, B. Majidi, M. Ezoddin, Application of modified nano-$\gamma$-alumina as an efficient adsorbent for removing malachite green (MG) from aqueous solution, Desal. Water Treat., 54 (2015) 758–768.
[24] B. Karunanithi, S.K. Kannaiyan, K. Balakrishnan, S. Muralidharan, G. Gopi, Adsorption of brilliant blue and malachite green by nano-graphene exfoliated from waste batteries, Chem. Eng. Technol., 44 (2021) 1877–1889.
[25] L. Wang, C. Shi, L. Pan, X. Zhang, J.-J. Zou, Rational design, synthesis, adsorption principles and applications of metal oxide adsorbents: a review, Nanoscale, 12 (2020) 4790–4815.
[26] M.A. Bekhti, M.S.E. Belardja, M. Lafjah, F. Chouli, A. Benyoucef, Enhanced tailored of thermal stability, optical and electrochemical properties of PANI matrix containing $Al_2O_3$ hybrid materials synthesized through in situ polymerization, Polym. Compos., 42 (2021) 6–14.
[27] A. Eltaweil, H.A. Mohamed, E.M. Abd El-Monaem, G. El-Subruiti, Mesoporous magnetic biochar composite for enhanced adsorption of malachite green dye: characterization, adsorption kinetics, thermodynamics and isotherms, Adv. Powder Technol., 31 (2020) 1253–1263.
[28] J. El Gaayda, R.A. Akbour, F.E. Titchou, H. Afanga, H. Zazou, C. Swanson, M. Hamdani, Uptake of an anionic dye from aqueous solution by aluminum oxide particles: equilibrium, kinetic, and thermodynamic studies, Groundwater Sustainable Dev., 12 (2021) 100540, doi: 10.1016/j.gsd.2020.100540.
[29] M. Aazza, H. Moussout, R. Marzouk, H. Ahlafi, Kinetic and thermodynamic studies of malachite green adsorption on alumina, J. Mater., 8 (2017) 2694–2703.
[30] S. Banerjee, S. Dubey, R.K. Gautam, M.C. Chattopadhyaya, Y.C. Sharma, Adsorption characteristics of alumina nanoparticles for the removal of hazardous dye, Orange G from aqueous solutions, Arabian J. Chem., 12 (2019) 5339–5354.
[31] A. Wasti, M. Ali Awan, Adsorption of textile dye onto modified immobilized activated alumina, J. Assoc. Arab Univ. Basic Appl. Sci., 20 (2016) 26–31.

[32] A.O. Adesina, O.A. Elvis, N.D. Mohallem, S.J. Olusegun, Adsorption of Methylene blue and Congo red from aqueous solution using synthesized alumina–zirconia composite, Environ. Technol., 42 (2021) 1061–1070.
[33] N. Mozaffari, N. Mozaffari, S.M. Elahi, S. Vambol, V. Vambol, N.A. Khan, N. Khan, Kinetics study of CO molecules adsorption on $Al_2O_3$/zeolite composite films prepared by roll-coating method, Surf. Eng., 37 (2021) 390–399.
[34] S. Oukil, F. Bali, D. Halliche, Adsorption and kinetic studies of methylene blue on modified HUSY zeolite and an amorphous mixture of γ-alumina and silica, Sep. Sci. Technol., 55 (2020) 2642–2658.
[35] A.S. Yusuff, J.O. Owolabi, C.O. Igbomezie, Optimization of process parameters for adsorption of heavy metals from aqueous solutions by alumina-onion skin composite, Chem. Eng. Commun., 208 (2021) 14–28.
[36] A. Baranik, R. Sitko, A. Gagor, B. Zawisza, Alumina/nano-graphite composite as a new nanosorbent for the selective adsorption, preconcentration, and determination of chromium in water samples by EDXRF, Anal. Bioanal. Chem., 410 (2018) 7793–7802.
[37] A. Bettayeb, B. Reguig, Y. Mouchaal, A. Yahiaoui, M. Chehimi, Y. Berredjem, Adsorption of metribuzin herbicide on raw maghnite and acid-treated maghnite in aqueous solutions, Desal. Water Treat, 145 (2019) 262–272.
[38] A. Zehhaf, A. Benyouncef, C. Quijada Tomás, S. Taleb, E. Morallon, Kinetic and thermodynamic study of the adsorption of As(III) from aqueous solutions by naturally occurring and modified montmorillonites, Biointerface Res. Appl. Chem., 2 (2012) 350–359.
[39] K.A. Rocky, A. Pal, T.H. Rupam, M.L. Palash, B.B. Saha, Recent advances of composite adsorbents for heat transformation applications, Therm. Sci. Eng. Prog., 23 (2021) 100900, doi: 10.1016/j.tsep.2021.100900.
[40] S. Pourshadlou, I. Mobasherpour, H. Majidian, E. Salahi, F. Shirani Bidabadi, C.-T. Mei, M. Ebrahimi, Adsorption system for $Mg^{2+}$ removal from aqueous solutions using bentonite/γ-alumina nanocomposite, J. Colloid Interface Sci., 568 (2020) 245–254.
[41] E.M. Kalhori, T.J. Al-Musawi, E. Ghahramani, H. Kazemian, M. Zarrabi, Enhancement of the adsorption capacity of the light-weight expanded clay aggregate surface for the metronidazole antibiotic by coating with MgO nanoparticles: studies on the kinetic, isotherm, and effects of environmental parameters, Chemosphere, 175 (2017) 8–20.
[42] B. Huang, C.H. Bartholomew, S.J. Smith, B.F. Woodfield, Facile solvent-deficient synthesis of mesoporous γ-alumina with controlled pore structures, Microporous Mesoporous Mater., 165 (2013) 70–78.
[43] M. Saeed, K. Farooq, M. Nafees, M. Arshad, M.S. Akhter, A. Waseem, Green and eco-friendly removal of mycotoxins with organo-bentonites; isothermal, kinetic, and thermodynamic studies, Clean–Soil Air Water, 48 (2020) 1900427, doi: 10.1002/clen.201900427.
[44] S. Banerjee, S. Dubey, R.K. Gautam, M. Chattopadhyaya, Y.C. Sharma, Adsorption characteristics of alumina nano-particles for the removal of hazardous dye, Orange G from aqueous solutions, Arabian J. Chem., 12 (2019) 5339–5354.
[45] K.S. Sing, Reporting physisorption data for gas/solid systems with special reference to the determination of surface area and porosity (Recommendations 1984), Pure Appl. Chem., 57 (1985) 603–619.
[46] J.C.P. Broekhoff, Mesopore determination from nitrogen sorption isotherms: Fundamentals, scope, limitations, Stud. Surf. Sci. Catal., 3 (1979) 663–684.
[47] Z.A. ALOthman, A review: fundamental aspects of silicate mesoporous materials, Materials, 5 (2012) 2874–2902.
[48] B. Yahyaei, S. Azizian, A. Mohammadzadeh, M. Pajohi-Alamoti, Preparation of clay/alumina and clay/alumina/Ag nanoparticle composites for chemical and bacterial treatment of waste water, Chem. Eng. J., 247 (2014) 16–24.
[49] T.S. Kazeem, S.A. Lateef, S.A. Ganiyu, M. Qamaruddin, A. Tanimu, K.O. Sulaiman, S.M.S. Jillani, K. Alhooshani, Aluminium-modified activated carbon as efficient adsorbent for cleaning of cationic dye in wastewater, J. Cleaner Prod., 205 (2018) 303–312.
[50] J.D. Clogston, A.K. Patri, Zeta Potential Measurement, S.E. McNeil, Ed., Characterization of Nanoparticles Intended for Drug Delivery, Humana Press, Totowa, NJ, 2011, pp. 63–70.
[51] M.H. Abu Elella, E.S. Goda, H. Gamal, S.M. El-Bahy, M.A. Nour, K.R. Yoon, Green antimicrobial adsorbent containing grafted xanthan gum/$SiO_2$ nanocomposites for malachite green dye, Int. J. Biol. Macromol., 191 (2021) 385–395.
[52] M. Kim, N. Sharma, J. Chung, K. Yun, Activated graphene with fractal structure for the adsorption of malachite green with high removal rate, Microporous Mesoporous Mater., 322 (2021) 111166, doi: 10.1016/j.micromeso.2021.111166.
[53] C. Belhajjia, A. Abid, A. Msaad, Z. Labaali, A. Zouhri, Synthesis, characterization and adsorption of Malachite green dye using novel materiel produced from opuntia ficus indica, Mater. Today:. Proc., 37 (2021) 4001–4006.
[54] R. Elmoubarki, F. Mahjoubi, H. Tounsadi, J. Moustadraf, M. Abdennouri, A. Zouhri, A. El Albani, N. Barka, Adsorption of textile dyes on raw and decanted Moroccan clays: kinetics, equilibrium and thermodynamics, Water Resour. Ind., 9 (2015) 16–29.
[55] Y.-C. Lee, J.-Y. Kim, H.-J. Shin, Removal of malachite green (MG) from aqueous solutions by adsorption, precipitation, and alkaline fading using talc, Sep. Sci. Technol., 48 (2013) 1093–1101.
[56] M.A. Adebayo, J.I. Adebomi, T.O. Abe, F.I. Areo, Removal of aqueous Congo red and malachite green using ackee apple seed–bentonite composite, Colloid Interface Sci. Commun., 38 (2020) 100311, doi: 10.1016/j.colcom.2020.100311.
[57] K. Thirumoorthy, S.K. Krishna, Removal of cationic and anionic dyes from aqueous phase by Ball clay – manganese dioxide nanocomposites, J. Environ. Chem. Eng., 8 (2020) 103582, doi: 10.1016/j.jece.2019.103582.
[58] W. Li, Z. Xie, S. Xue, H. Ye, M. Liu, W. Shi, Y. Liu, Studies on the adsorption of dyes, Methylene blue, Safranin T, and Malachite green onto polystyrene foam, Sep. Purif. Technol., 276 (2021) 119435, doi: 10.1016/j.seppur.2021.119435.
[59] M.S. Derakhshan, O. Moradi, The study of thermodynamics and kinetics methyl orange and malachite green by SWCNTs, SWCNT-COOH and SWCNT-$NH_2$ as adsorbents from aqueous solution, J. Ind. Eng. Chem., 20 (2014) 3186–3194.
[60] R. Haounati, H. Ouachtak, R. El Haouti, S. Akhouairi, F. Largo, F. Akbal, A. Benlhachemi, A. Jada, A.A. Addi, Elaboration and properties of a new SDS/CTAB@Montmorillonite organoclay composite as a superb adsorbent for the removal of malachite green from aqueous solutions, Sep. Purif. Technol., 255 (2021) 117335, doi: 10.1016/j.seppur.2020.117335.
[61] F. Zhang, B. Ma, X. Jiang, Y. Ji, Dual function magnetic hydroxyapatite nanopowder for removal of malachite green and Congo red from aqueous solution, Powder Technol., 302 (2016) 207–214.
[62] J.O. Ojediran, A.O. Dada, S.O. Aniyi, R.O. David, Functionalized *Zea mays* cob (FZMC) as low-cost agrowaste for effective adsorption of malachite green dyes data set, Chem. Data Collect., 30 (2020) 100563, doi: 10.1016/j.cdc.2020.100563.
[63] E.C. Lima, F. Sher, A. Guleria, M.R. Saeb, I. Anastopoulos, H.N. Tran, A. Hosseini-Bandegharaei, Is one performing the treatment data of adsorption kinetics correctly?, J. Environ. Chem. Eng., 9 (2021) 104813, doi: 10.1016/j.jece.2020.104813.
[64] M. Choudhary, R. Kumar, S. Neogi, Activated biochar derived from *Opuntia ficus-indica* for the efficient adsorption of malachite green dye, $Cu^{+2}$ and $Ni^{+2}$ from water, J. Hazard. Mater., 392 (2020) 122441, doi: 10.1016/j.jhazmat.2020.122441.
[65] J.S. Piccin, T.R.S.A. Cadaval Jr., L.A.A. de Pinto, G.L. Dotto, Adsorption Isotherms in Liquid Phase: Experimental, Modeling, and Interpretations, A. Bonilla-Petriciolet, D. Mendoza-Castillo, H. Reynel-Ávila, Eds., Adsorption Processes for Water Treatment and Purification, Springer, Cham, 2017, pp. 19–51.
[66] M.E. González-López, C.M. Laureano-Anzaldo, A.A. Pérez-Fonseca, M. Arellano, J.R. Robledo-Ortíz, A critical overview

of adsorption models linearization: methodological and statistical inconsistencies, Sep. Purif. Rev., 51 (2022) 358–372.
[67] M.A. Al-Ghouti, D.A. Da'ana, Guidelines for the use and interpretation of adsorption isotherm models: a review, J. Hazard. Mater., 393 (2020) 122383, doi: 10.1016/j.jhazmat.2020.122383.
[68] J. Zhu, Y. Wang, J. Liu, Y. Zhang, Facile one-pot synthesis of novel spherical zeolite–reduced graphene oxide composites for cationic dye adsorption, Ind. Eng. Chem. Res., 53 (2014) 13711–13717.
[69] Z. Shi, C. Xu, H. Guan, L. Li, L. Fan, Y. Wang, L. Liu, Q. Meng, R. Zhang, Magnetic metal organic frameworks (MOFs) composite for removal of lead and malachite green in wastewater, Colloids Surf., A, 539 (2018) 382–390.
[70] D. Datta, Ö. Kerkez Kuyumcu, Ş.S. Bayazit, M. Abdel Salam, Adsorptive removal of malachite green and Rhodamine B dyes on $Fe_3O_4$/activated carbon composite, J. Dispersion Sci. Technol., 38 (2017) 1556–1562.
[71] W. Qu, T. Yuan, G. Yin, S. Xu, Q. Zhang, H. Su, Effect of properties of activated carbon on malachite green adsorption, Fuel, 249 (2019) 45–53.
[72] F. Ali, S. Bibi, N. Ali, Z. Ali, A. Said, Z.U. Wahab, M. Bilal, H.M. Iqbal, Sorptive removal of malachite green dye by activated charcoal: process optimization, kinetic, and thermodynamic evaluation, Case Stud. Chem. Environ. Eng., 2 (2020) 100025, doi: 10.1016/j.cscee.2020.100025.
[73] E.C. Lima, A. Hosseini-Bandegharaei, J.C. Moreno-Piraján, I. Anastopoulos, A critical review of the estimation of the thermodynamic parameters on adsorption equilibria. Wrong use of equilibrium constant in the Van't Hoof equation for calculation of thermodynamic parameters of adsorption, J. Mol. Liq., 273 (2019) 425–434.
[74] H.-O. Chahinez, O. Abdelkader, Y. Leila, H.N. Tran, One-stage preparation of palm petiole-derived biochar: characterization and application for adsorption of crystal violet dye in water, Environ. Technolo. Innov., 19 (2020) 100872, doi: 10.1016/j.eti.2020.100872.
[75] P. Sharma, H. Laddha, M. Agarwal, R. Gupta, Selective and effective adsorption of malachite green and methylene blue on a non-toxic, biodegradable, and reusable fenugreek galactomannan gum coupled $MnO_2$ mesoporous hydrogel, Microporous Mesoporous Mater., (2022) 111982, doi: 10.1016/j.micromeso.2022.111982.
[76] H.N. Tran, Y.-F. Wang, S.-J. You, H.-P. Chao, Insights into the mechanism of cationic dye adsorption on activated charcoal: the importance of π–π interactions, Process Saf. Environ. Prot., 107 (2017) 168–180.
[77] L. Meng, X. Zhang, Y. Tang, K. Su, J. Kong, Hierarchically porous silicon–carbon–nitrogen hybrid materials towards highly efficient and selective adsorption of organic dyes, Sci. Rep., 5 (2015) 1–16.

## Supplementary information

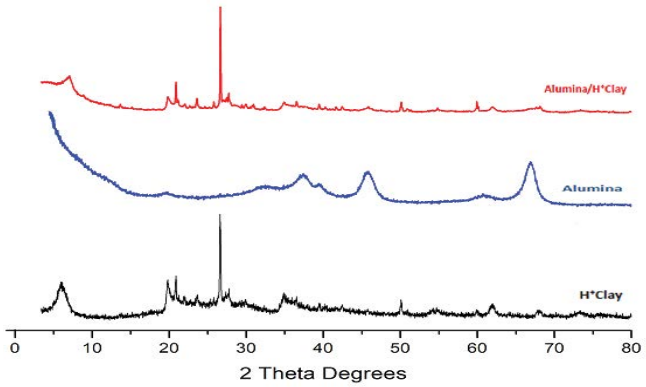


Fig. S1. XRD pattern of $H^+$Clay, Alumina and, Alumina/$H^+$Clay composite.

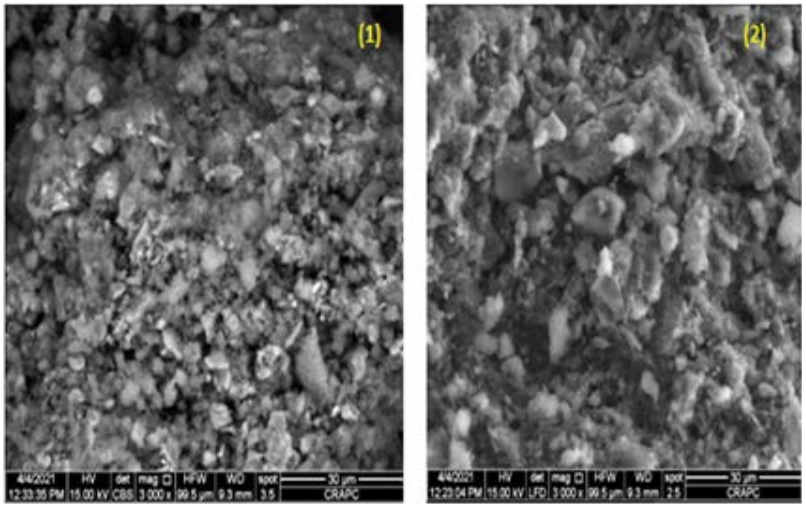


Fig. S2. SEM images of Alumina/$H^+$Clay composite before (1) and after (2) MG dye adsorption.